Optical Engineering

SPIEDigitalLibrary.org/oe

Developments of mid-infrared optical parametric oscillators for spectroscopic sensing: a review

Jiahui Peng

SPIE

Developments of mid-infrared optical parametric oscillators for spectroscopic sensing: a review

Jiahui Peng*
IMRA America Inc., 1044 Woodridge Avenue, Ann Arbor, Michigan 48105

Abstract. Optical parametric oscillator is an attractive way of generating tunable mid-infrared light in the spectral range where lasers simply do not exist—for the needs of spectroscopy, medical applications, remote sensing, etc. We will go through the fundamentals of the optical parametric oscillator first and then introduce the related new phase-matching, cavity design, and spectroscopic techniques. [DOI: 10.1117/1.OE.53.6.061613]

Keywords: mid-infrared laser; parametric process; frequency combs spectroscopy.

Paper 131363SSV received Sep. 3, 2013; revised manuscript received Jan. 3, 2014; accepted for publication Jan. 9, 2014; published online Feb. 27, 2014.

1 Introduction

An optical parametric oscillator (OPO) is a coherent light source similar to a laser, but based on the optical parametric amplification in a nonlinear crystal rather than the stimulated emission in a gain media. It was first achieved in 1965 by Giordmaine and Miller,[1] but theoretical works were even earlier.[2,3] A main attraction of OPOs is to generate widely tunable coherent radiation [e.g., in the mid-infrared (mid-IR), far-infrared, or terahertz spectral region), which are difficult or impossible to obtain from any laser. This makes OPOs very valuable for laser spectroscopy and its applications in sensing.[4]

The vibrational spectrum of a molecule is considered to be a unique physical property and is characteristic of the molecule even in a complexed environment.[5] For the specific mid-IR spectral region of 2 to 20 μm (500 to 5000 cm^{-1}), it is of great interest. A large number of molecules undergo strong characteristic vibrational transitions in this spectral region (Fig. 1). Mid-IR spectroscopy provides a powerful tool not only for understanding the structure of a molecule and its governing physical laws, but also for performing nonintrusive diagnostics of composite systems of physical, chemical, or biological interests, including isotopologues, in the gas, liquid, or solid phase.[6,7]

Furthermore, there are two important windows (3 to 5 μm and 8 to 13 μm) in the Earth's atmosphere that is relatively transparent. These regions can be exploited to detect small traces of environmental and toxic vapors down to the sensitivities of parts-per-billion (ppb) in a variety of atmospheric, astronomic, geophysical, security, and industrial applications. The low Rayleigh scattering losses in the mid-IR spectral region ($\propto \lambda^{-4}$) benefit tomography and imaging in turbid media.[7,9]

Within the last decade, the development of the optical frequency comb has allowed frequency and time measurements with previously unattainable precision, facilitated carrier-envelope phase stabilized lasers, and revolutionized the field of spectroscopy.[10–12] A mode-locked femtosecond laser gives a regular comb spectrum of millions of laser modes with a spacing equals to the pulse repetition frequency. Optical frequency combs in the visible and near-IR domains have enabled the development of new ultraprecise optical atomic clocks, and commercially available combs have become standard instruments of precision spectroscopy. They are now becoming enabling tools for many applications, ranging from the calibration of astronomical spectrograph to molecular spectroscopy. In the mid-IR range, the advent of femtosecond optical combs is expected not only to bring a new set of tools for precision spectroscopy, but also to allow spectroscopy to be explored in a broader sense. Precise investigations of changes in the composition of a molecular sample over a large dynamic range might also soon be within reach thanks to novel mid-IR frequency-comb-based techniques.

Mid-IR OPO shows great potentials in spectroscopy-related applications in sensing. Over the last few years, many research groups all over the world have done tremendous great works on this research. In this review, we will go through the fundamentals of the OPO first and then introduce some of those novel developments.

2 Fundamentals of OPO

Optical parametric amplification/oscillation belongs to a broader class of electromagnetic phenomena described within the framework of the general Maxwell equations. With the assumption of the absence of extraneous charges and currents, we can write the set of Maxwell equations in the form

$$\nabla \cdot \mathbf{D} = 0, \tag{1}$$

$$\nabla \cdot \mathbf{B} = 0, \tag{2}$$

$$\nabla \times \mathbf{E} = -\frac{\partial \mathbf{B}}{\partial t}, \tag{3}$$

*Address all correspondence to: Jiahui Peng, E-mail: jpeng@imra.com

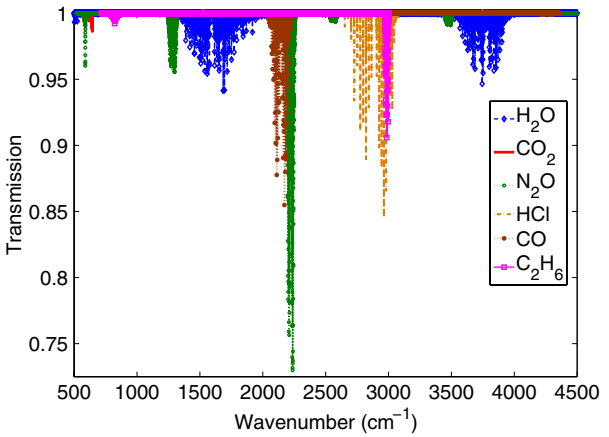

Fig. 1 HITRAN simulation of absorption bands of various molecules in the 500 to 5000 cm^{-1} spectral region.[8]

$$\nabla \times \mathbf{B} = \frac{\partial \mathbf{D}}{\partial t}. \tag{4}$$

The relationship between the electric flux density **D** and the electric field **E** depends on the electric properties of the medium, which are characterized by the polarization density **P**.

$$\mathbf{D} = \epsilon_0 \mathbf{E} + \mathbf{P}. \tag{5}$$

We take the curl of the curl-**E** Maxwell equation [Eq. (3)] and interchange the order of space and time derivatives on the right-hand side of the resulting equation. With knowing that $\nabla \times \nabla \times \mathbf{E} = \nabla(\nabla \cdot \mathbf{E}) - \nabla^2 \mathbf{E}$, we obtain

$$\nabla^2 \mathbf{E} - \frac{1}{c^2}\frac{\partial^2 \mathbf{E}}{\partial t^2} = \frac{1}{\epsilon_0 c^2}\frac{\partial^2 \mathbf{P}}{\partial t^2}. \tag{6}$$

It is often convenient to split **P** into a linear and a nonlinear part (with subscripts of L and NL, respectively): $\mathbf{P} = \mathbf{P}_{\mathrm{L}} + \mathbf{P}_{\mathrm{NL}}$. By introducing ϵ_1, a complex frequency-dependent dielectric tensor, we can rewrite Eq. (6) as

$$\nabla^2 \mathbf{E} - \frac{\epsilon_1}{c^2}\frac{\partial^2 \mathbf{E}}{\partial t^2} = \frac{1}{\epsilon_0 c^2}\frac{\partial^2 \mathbf{P}_{\mathrm{NL}}}{\partial t^2}. \tag{7}$$

When $\mathbf{P}_{\mathrm{NL}} = 0$, Eq. (7) describes the light propagating in a dissipative medium but without any cross-talking of different frequency components of the light. However, if $\mathbf{P}_{\mathrm{NL}} \neq 0$, we start to see more interesting nonlinear effects. For a more rigid derivation of Eq. (7), readers can find details in Refs. 13 to 15, and here we concentrate on the OPO only.

In a typical OPO, a shorter-wavelength laser pumps the second-order nonlinear susceptibility of a suitable optical material, introducing of $\mathbf{P}_{\mathrm{NL}}$, to generate lower-frequency components. Combined with an appropriate resonator for optical feedback, oscillation can be established at one or more wavelengths, called single or multiple resonant OPO (see Sec. 4). The oscillation wavelength is often tuned by adjusting the parameters of the resonator or the nonlinear material, e.g., the orientation and temperature of the nonlinear material.

Let us now consider the situation shown in Fig. 2, in which optical waves at frequencies ω_p and ω_s interact in

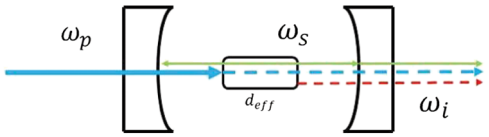

Fig. 2 A typical optical parametric oscillator: pump laser ω_p pumps the nonlinear crystal d_{eff}. The signal beam ω_s is resonant, whereas the idler ω_i is ejected by the resonator mirrors. However, cavity can also be designed to resonant with pump laser and idler beam too (Sec. 4).

a lossless nonlinear optical medium and produce an output wave at the difference frequency $\omega_i = \omega_p - \omega_s$, where ω is frequency; in this whole paper, subscripts p, s, and i stand for pump, signal, and idler, respectively. For a fixed polarization and propagation geometry, it is possible to express the nonlinear polarization for OPO/OPA system as a scalar relationship $\mathrm{P}_{\mathrm{NL}}(\omega_p) = 4\epsilon_0 d_{\mathrm{eff}} E(\omega_i) E(\omega_s)$ (d_{eff} is the effective nonlinearity). If the applied fields are linear polarized and propagate along z direction, we can represent the applied fields as

$$E_p(z,t) = A_p(z,t)e^{i(k_p z - w_p t)} + c.c.,$$
$$E_i(z,t) = A_i(z,t)e^{i(k_i z - w_i t)} + c.c.,$$
$$E_s(z,t) = A_s(z,t)e^{i(k_s z - w_s t)} + c.c.$$

Here, we already take into account the cases when the applied fields are pulses (A is the envelope amplitude of the field). At the same time, we can approximate the wave vector as a Taylor expansion: $k = k^0 + k'(\omega - \omega_0) + 1/2k''(\omega_0 - \omega)^2$, $k' = dk/d\omega = 1/v_g$, where v_g is the group velocity and k'' is the group velocity dispersion. As we all know, the requirement for such expansion is the quantity $|\omega_0 - \omega| \ll \omega_0$. However, it is still valid for broad bandwidth femtosecond pulses in many cases.[16] By applying slowly varying envelope approximation ($|d^2A/dz^2| \ll |kdA/dz|$), we can obtain the coupled-wave equations for OPA as

$$\left[\frac{dA_p}{dz} + k_p'\frac{dA_p}{dt} + \frac{1}{2}ik_p''\frac{d^2A_p}{dt^2}\right]e^{ik_p z} = \frac{2id_{\mathrm{eff}}\omega_p^2}{k_p c^2}A_s A_i e^{i(k_s+k_i)z}, \tag{8}$$

$$\left[\frac{dA_s}{dz} + k_s'\frac{dA_s}{dt} + \frac{1}{2}ik_s''\frac{d^2A_s}{dt^2}\right]e^{ik_s z} = \frac{-2id_{\mathrm{eff}}\omega_s^2}{k_s c^2}A_p A_i^* e^{i(k_p-k_i)z}, \tag{9}$$

$$\left[\frac{dA_i}{dz} + k_i'\frac{dA_i}{dt} + \frac{1}{2}ik_i''\frac{d^2A_i}{dt^2}\right]e^{ik_i z} = \frac{-2id_{\mathrm{eff}}\omega_i^2}{k_i c^2}A_p A_s^* e^{i(k_p-k_s)z}. \tag{10}$$

It is easy to see there is an oscillating term of $e^{\pm i(k_s+k_i-k_p)z}$, which gives the phase-matching condition. When the phase-matching condition is fulfilled $\Delta k = k_s + k_i - k_p = 0$, the individual atomic dipoles that constitute the material system are properly phased so that the field

emitted by each dipole adds coherently in the propagation direction. The total power radiated by the ensemble of atomic dipoles thus scales as the square of the number of atoms that participate, and the signal and idler extract energy most efficiently from the pump laser.[14] As the requirement of $\omega_p = \omega_i + \omega_s$ is regarded as the energy conservation, the requirement of phase-matching can be viewed as the momentum conservation.

The coupling equations can be solved analytically with various initial conditions.[17] For simplicity and practicality, we can neglect pump field depletion ($dA_p/dz = 0$) and assume the presence of no idler in the beginning of parametric process $A_i(z = 0) = 0$. The single-pass fractional gain in signal intensity ($I = (1/2)\epsilon_0 nc|A|^2$) is[18,19]

$$G_s(l) = \frac{I_s(z = l)}{I_s(z = 0)} - 1 = \Gamma^2 l^2 \frac{\sinh^2(gl)}{(gl)^2}, \tag{11}$$

where l is the length of the nonlinear medium, Γ is the parametric gain factor given by

$$\Gamma = \sqrt{\frac{2\omega_s\omega_i|d_{\text{eff}}|^2 I_p}{n_p n_s n_i \epsilon_0 c^3}}, \tag{12}$$

and g is the total gain factor given by

$$g = \sqrt{\Gamma^2 - \left(\frac{\Delta k}{2}\right)^2}. \tag{13}$$

The parametric gain depends on the intensity of the pump laser, as well as on the material, e.g., nonlinear coefficient, refractive index, and the interaction length. However, the phase-matching condition plays a very important role if not the most.[20]

3 Phase-Matching at Mid-IR

Due to the dispersion, the pump, signal, and idler have different phase velocities. The relative phase of the interactive waves varies along the medium. A measure of the phase mismatch is the coherence length $L_c = |\pi/\Delta k|$, which defines the distance over which the relative phase of the interacting waves shifts by π. The propagation beyond the coherence length, which is typically several micrometers, leads to the energy back-conversion from the generated waves into the pump wave.[20]

However, the phase-matching can be achieved by making use of the birefringence: choosing the orientation of the crystal so that the pump laser (highest frequency) propagates along the fast axis (smaller refraction index) and the signal and idler propagate along the slow axis (larger refraction index).[21] The process is called type I phase-matching when both signal and idler have the same polarization perpendicular to that of the pump laser. For type II phase-matching, the polarization of the signal and idler are perpendicular to each other.[14,20,22,23] In most literatures, the phase-matching is explained by using the uniaxial crystal and giving a series of combinations. Those combinations are meaningless for biaxial crystals, but the principle is same. This phase-matching achieved by tuning crystal angles is sometimes called critical phase-matching. The attribute critical comes from the fact that this technique is relatively sensitive to the misalignment of the three beams.[22] A consequence of critical phase-matching is the spatial walk-off generated by the birefringence, which reduces the interaction length of the optical waves. It can be compensated via a noncollinear geometry.[23–25] A major advantage of critical phase matching is that the crystal temperature can often be close to room temperature, so that a crystal oven is not required.

On the other hand, this birefringence can be fulfilled by changing the temperature of the nonlinear crystal: noncritical phase-matching.[26,27] Noncritical phase-matching is sometimes called temperature phase-matching or 90 deg phase-matching. The interacting beams are aligned such that they propagate along same axis of the birefringent nonlinear crystal. The phase-matching is achieved by adjusting the crystal temperature such that the phase velocities of the interacting waves are equal (polarizations are adjustable parameters, too). It results in the absence of spatial walk-off and less angular sensitivity, which is important in applications with tight focusing. As shown in Eq. (11), the gain is proportional to the intensity; therefore, the conversion efficiency can often be higher with noncritical phase-matching because of the tight focusing. At the same time, the crystal temperature is usually somewhat above room temperature, so that a temperature-stabilized crystal oven is required, which protects those crystals from being deliquescence.

Many nonlinear crystals are frequently used for mid-IR OPO,[23] and some of them are listed in Table 1.

However, there are limits to utilize the birefringence of an optical material to achieve the phase-matching. First, not all nonlinear materials may possess birefringence (e.g., isotropic semiconductors zinc selenide and gallium arsenide), or may possess sufficient birefringence to compensate for the dispersion of the linear refractive index over the wavelength range of interest. Second, sometimes nonlinearity is low or 0 under the phase-matching condition (d_{eff} varies

Table 1 Frequently used nonlinear crystals for mid-IR optical parametric oscillators.

Crystal	Spectral regions (μm)	References
Lithium niobate ($LiNbO_3$)	0.35 to 5.2	27, 28
Potassium titanyl phosphate (KTP)	0.35 to 4.5	29 to 31
$KTiOAsO_4$ (KTA)	0.35 to 5.5	32 to 34
β-barium borate (BBO)	0.19 to 3.3	35
Lithium triborate (LBO)	0.16 to 2.6	36
Zinc germanium diphosphide (ZGP)	0.7 to 12	37, 38
Silver gallium sulfide and selenide ($AgGaS_2$ and $AgGaSe_2$)	0.5 to 13.2/0.78 to 18	39, 40
Cadmium selenide (CdSe)	0.75 to 25	41
$LiGaS_2$, $LiGaSe_2$, and $LiGaTe_2$	0.33 to 12/0.38 to 14/0.52 to 15	42

with the orientation of a crystal). These difficulties led researchers to find a way to achieve phase-matching by periodically altering the sign of the nonlinear coefficient, so-called quasi-phase-matching (QPM).[43,44] The relative phase between the three waves is corrected using a periodic change in the sign of the nonlinear susceptibility before the back-conversion starts.[14]

$$d(z) = d_{\text{eff}}\,\text{sign}[\cos(2/\Lambda)], \tag{14}$$

where Λ is the period of the alternation of the crystalline. This spatial modulation causes a phase mismatching $\Delta k_Q = k_s + k_i - k_p - 2\pi/\Lambda$.[14,44] The optimized phase-matching condition can be achieved if

$$\Lambda = 2\pi/(k_s + k_i - k_p) = 2L_c. \tag{15}$$

Although the technique of QPM (Fresnel QPM) was proposed in 1962 (Ref. 43) and demonstrated in 1965,[45] difficulties in fabrication of the periodic structure in the range of the coherence length (typically 1 to 100 μm) have prevented its realization. The relative phase shift experienced at total internal reflection is used to reset the relative phases between interacting waves.[46–48]

The advances in the fabrication of structured ferroelectrics, meanwhile, have established this technique for efficient frequency-conversion applications.[49,50]

QPM offers two major advantages over birefringence phase-matching. First, the polarization of the interacting waves can be same. This allows the use of the largest d_{eff} coefficient of the crystal, which reduces the pump threshold and increases the conversion efficiency.[14,20] The second advantage is that the QPM of any combination of pump, signal, and idler wavelength can be realized in such materials. In addition, QPM provides design flexibility of nonlinear conversion devices by engineered domain structures.[20] The most challenging aspect of the fabrication is the periodic nonlinear structure. This may be accomplished by lithographically exposing the crystal to a periodic electric field that reverses the direction of the crystal's permanent electric polarization, a technique called poling. This approach has been applied to ferroelectric crystals, such as $LiTaO_3$, potassium titanyl phosphate, and $LiNbO_3$; the latter has spawned a technology known as periodically poled lithium niobate.[51] Nowadays, people can have highly efficient OPO operate at continuous-wave (CW) with low threshold.[52]

The zincblende semiconductors, such as GaAs, ZnSe, and GaP, have large nonlinear susceptibilities and low optical absorption into the mid-IR spectral region. They have long been used for mid-IR nonlinear optics. As pointed out above, their optical isotropy, a consequence of their cubic crystal structure, precludes birefringent phase-matching.[53] The QPM really gives an opportunity to apply these high-nonlinearity crystals in mid-IR spectral region.

A number of QPM techniques based on stacks of crystal plates with alternating orientation have been explored, but fabrication has proved to be challenging.[53–57] The best way to fabricate stacked-plate is to have crystal plates being diffusion-bonded to each other. Diffusion bonding consists of carefully polishing, cleaning, and placing. To avoid the localized scattering losses and a constant Λ, it requires very high fabricating performance.

The difficulty in fabricating suitable stacks of plates for QPM suggests that a monolithic structure would be more applicable. Epitaxial growth of orientation-patterned materials, with lithographically controlled patterns, has greatly opened the range of applicability of QPM.[53,58] In template controlled growth, a substrate is patterned lithographically such that the orientation of subsequently grown films is controlled by the pattern on the substrate. Multilayer, thin-film growth on such a template, for example, by molecular-beam epitaxy or organometallic vapor-phase epitaxy, can produce a QPM waveguide device, while thick-film growth on the template, for example, by hydride vapor-phase epitaxy, can produce a bulk (millimeter-thick) film for QPM interactions.[53]

Now, people obtained high efficiency OPO with an orientation-patterned (OP) GaAs with tuning range covering from 2 to 9 μm.[59,60] A major constraint of OPGaAs-based OPO is the strong two-photon absorption, which limits the pump of OPGaAs with wavelengths longer than ~1.8 μm.[61] Lasers operating at this wavelength (2 μm), like the Tm,Ho:YLF laser, are preferable for their relative simplicity.[62–64] With such femtosecond thulium fiber laser as pump source, broadband mid-IR OPO can be achieved. Output bandwidth covers from 2.6 to 6.1 μm at the 30 dB level[65] and can be applied to the carrier-envelope offset (CEO) frequency measurements. In one such measurement, the authors show that the CEO frequency of the synchronously pumped OPO signal wave is a linear function of the CEO frequency of the pump laser, with a slope determined by the signal to pump center-frequency ratio.[66]

Other than the phase-matching techniques mentioned above, very recently people found the random motion of the relative phases in highly transparent polycrystalline materials can be an effective strategy for achieving efficient phase-matching in isotropic materials.[67] The back-conversion of signal and idler to pump is a result of an interference effect between the three coherent lights. Such interference could be destroyed if the waves were allowed to lose their respective phases randomly in the material, in that the nonlinear susceptibility does not average to zero. Because of the random phase, it leads to a coherent growth of the nonlinear generated fields according to $\sqrt{N}$, where N is the number of the microcrystallite.[67] Both the theoretical work and the experimental work show that the second-order nonlinear generation of light is also possible in structures of randomly oriented nonlinear domains,[68] which could be useful for the OPA process in the future.

4 Architecture of OPO

As discussed in Sec. 1, OPO operates like a laser. It requires the same three elements of a laser: pump source, cavity, and gain media. Output of the OPO ranges from CW to femtosecond pulses. The design and performance of OPOs have a huge variety. The design of the cavity is strongly connected to the output characteristic of the pump source and the phase-matching condition. Three types of resonators are distinguished depending on the number of resonating waves.[20,22]

The singly resonant OPO (SRO) has highly reflecting mirrors at either the signal or the idler light, and dichroic resonator mirrors or some polarizing optics are used to make high resonator losses for the nonresonant lights, so that there is very little optical feedback. In principle, this configuration is of particular importance in providing

continuous wavelength tunability since it gives less restriction on the cavity. It also has a high stability and a narrow linewidth output.[69,70] However, the disadvantage of the SRO is the losses of the other lights. From the coupling equation discussed above, we can see that the SRO will require higher pump power and has higher oscillation threshold. With the help of high quality of optics, novel cavity configurations, and crystals, people have made highly efficient CW mid-IR OPOs, and the threshold has been reduced from a couple watts to several hundred milliwatts.[71–75]

For doubly resonant OPO (DRO) configurations where both signal and idler waves are resonated, the threshold could be reduced by one to three orders of magnitude.[20] As the DRO is overconstrained by the requirements of energy conservation, phase-matching, and simultaneous resonance of signal and idler waves, perturbations on the pump frequency or OPO cavity length can cause large power fluctuations and mode hopping of the DRO.[20,76] However, these problems can be overcome by using frequency-stable, single-mode lasers.[77,78] The doubly resonant configuration where pump and signal (or idler) are resonated is called pump-enhanced SRO and provides a compromise between the low threshold of DROs and the wide tunability of SROs.[20,79]

Triply resonant OPOs suffer from the combined problems of both types of DROs with smaller tunability in comparison to SRO, but they offer lowest threshold (can be seen from the coupling equations) in the range of several milliwatts or less.[20,80,81]

For the new developments of OPOs at CW, nanosecond, and femtosecond different pulse durations, readers can find more details in Refs. 82 and 83.

All the OPOs talked above rely on nonlinear crystals placed into external cavities and pumped by powerful external lasers. They tend to be relatively complex and large devices that are difficult to align and miniaturize, so great efforts have been devoted to develop integrated devices. Recently, researchers reported a monolithic semiconductor triple microcavity OPO with signal, pump, and idler waves propagating along the vertical direction of the nanostructure. The pump threshold is low enough to envisage the realization of an all-semiconductor electrically pumped microparametric oscillator.[84] There are efforts being made to combine an OPO with a microcavity to generate mid-IR frequency combs too.[85]

Another idea is to make use of backpropagation wave to achieve effective OPO, which was first proposed in 1966.[86] In that initial study, birefringence in the nonlinear crystal was used, and it was only applicable to the case where the idler frequency was in the far-IR region. In 2007, the first experiment of mirrorless OPO was conducted, and it was fullfiled via QPM.[87] This counterpropagating parametric interaction, where the signal and idler waves propagate in opposite directions, puts much stronger constraints on the momentum mismatch, thus promising much better control over the spectrum. These unique properties open up possibilities for broadband pulse generation in the near-IR or mid-IR regions, and for tuning a narrow band mid-IR idler wave with high precision.[87,88]

5 Sensing Applications of Mid-IR OPO

As mentioned in the Introduction, mid-IR OPO is an important coherent light source for molecular spectroscopy and it provides sensitivity and selectivity.

The fact that molecules absorb light at distinct, characteristic wavelengths allows for the unique spectral identification of a chemical by measuring its absorption spectrum. With the development of OPOs, it has become increasingly important to use OPO as a tunable coherent light source to monitor and detect trace gases in diverse fields ranging from pollution and greenhouse-gas emission, to applications involving environmental control for the workplace and space habitats.[4,89,90] Trace gas detection using a CW tunable SRO was reported to have an ethane detection sensitivity <1 ppb, which was close to the best values achieved with conventional method.[91] Compact OPO system was also used for remote sensing explosives vapor detection at ppb level.[92]

Other than conventional absorption spectroscopy, there are many new spectroscopic technologies developed, especially the frequency combs technique.[10,12] Mid-IR OPO shows great advantages in a new very sensitive absorption spectroscopy technique, called cavity-ring-down spectroscopy. Instead of measuring the small difference between the incident and transmitted radiation power in conventional absorption spectroscopy, this technique measures the number of cavity round-trip times after which the power has dropped to $1/e$ of its initial value.[20,93–95]

The direct frequency comb spectroscopy directly employs optical frequency combs to probe spectral features in a massively parallel probing in the frequency domain with a comb bandwidth spanning tens to hundreds of terahertz.[96] It also allows time-resolved studies of coherent and incoherent dynamics. Femtosecond OPO provides high-power frequency combs in the mid-IR spectral region and fits very well for these applications.[97,98] These OPOs can operate both for broad band width and widely tunable applications.[99,100]

Cavity-enhanced direct frequency comb spectroscopy (CE-DFCS) emerged as a powerful new technique that provides high spectral coverage, high resolution, and high sensitivity by combining the frequency comb with several other important elements, including an external enhancement cavity and a broadband, yet highly resolving, detection system.[101–103] This enhanced spectroscopy technique can be applied to breath analysis, a medical diagnostics demonstrating that some molecules in the breath are potential markers for certain diseases.[104] Using intracavity spectroscopy of broadband OPO, researchers achieved ultrasensitive detection of methane, isotopic carbon dioxide, carbon monoxide, formaldehyde, acetylene, and ethylene as well.[105]

Thanks to the precision spectroscopy, spectral shifts of transition frequencies associated with different isotopes can be detected. The determination of isotope ratios has proved to be a powerful tool in medical analysis, geology, and climate research. Stable isotopes of H_2O, CO_2, and O_2 are analyzed in ice cores to track the history of the Earth's climate. They are also used for atmospheric studies and to observe groundwater transport. A precise measurement conducted with mid-IR OPO of the ratio of the two stable carbon isotopes of CO_2 ($^{13}CO_2$and $^{12}CO_2$) can provide valuable information about CO_2 exchange processes in the volcanic plume.[106,107]

The invention of the femtosecond frequency comb really made revolutions in the field of spectroscopy. Besides the newly developed techniques discussed above, dual frequency comb spectroscopy (DFCS) emerges as a promising, highly sensitive, and superior fast spectroscopy with high

resolution to complement the traditional Fourier transform spectroscopy (FTS). In dual-comb spectroscopy, two frequency combs with slightly different line spacings are heterodyned after passing through the cell, yielding a downconverted radio frequency comb that contains information on the absorption experienced by both combs.[7,108,109] Compared to traditional FTS, DFCS is extremely fast. A fast oscilloscope can display an interferogram and the broadband spectrum by fast Fourier transform in real time. The signal record then can be transformed to a spectrum with high resolution at high signal-to-noise ratio, and part-per-billion detection limits was achieved for several important molecules, including methane, ethane, isoprene, and nitrous oxide.[110,111] Instead of using two frequency-locked OPOs as the dual-comb source, a dual-comb source is comprised of a single synchronously pumped OPO driven by two independent lasers and capable of producing two mid-IR pulses sequences.[112]

The combination of frequency combs with a Fabry-Perot filtering cavity is a promising approach to achieve high Doppler shift resolution via the spectrograph wavelength calibration. This high resolution can be used to search for extrasolar planets and to observe in real time the evolution of the cosmological redshift of distant objects, called as astro-comb technique, and OPO offers the freedom of both important parameters: the optical frequency and the repetition rate.[113–115]

Based on the frequency combs, a coherent anti-Stokes Raman spectroscopy system was developed to perform spectroscopic imaging over a broad spectral bandwidth within a few microseconds.[116] OPOs are perfect tools to generate suitable frequency combs for various spectral regions and further to extend its applications.

6 Discussions

A novel technique is achieved to generate mode-locked pulses from a CW OPO.[117] This technique is based on the deployment of an amplitude/phase modulator in combination with a CW OPO, simultaneously providing spectral broadening and nonlinear parametric gain.[117,118] This approach could enable the generation of tunable ultrashort pulses in the mid-IR spectral regions using OPOs directly pumped by CW lasers.

Another new frequency comb generation principle has emerged that uses parametric frequency conversion in high resonance quality factor microresonators. This approach provides access to generate high repetition rate frequency combs through compact system, chip-scale integration, and benifit a number of comb applications, such as in astronomy, microwave photonics, or telecommunications.[85,119]

Mid-IR OPOs also have great potential in biomedical applications. Not only their tunable wavelength systems can be used for the imaging of bio-samples, but also their ablation capability can be used for clinic surgical applications.[120,121]

Thanks to the new nonlinear crystals, improved optics components, and new spectroscopy techniques, the applications of OPOs have been significantly extended in the last 10 years. We would expect that the sensing related application will be further improved in the future, especially with the trace gas detection and biomedical-related imaging process. With the boosts of these applications, the size of OPOs will be further reduced and the performance of them will be further improved as well.

Acknowledgments

The author acknowledges Dr. F. Zhu who provided the script for plotting Fig. 1.

References

1. J. A. Giordmaine and R. C. Miller, "Tunable coherent parametric oscillation in LiNbO3 at optical frequencies," *Phys. Rev. Lett.* **14**(24), 973–96 (1965).
2. R. H. Kingston, "Parametric amplification and oscillation at optical frequencies," *Proc. IRE* **50**, 472–474 (1962).
3. A. E. Siegman, "Nonlinear optical effects: an optical power limiter," *Appl. Opt.* **1**(S1), 127–132 (1962).
4. F. K. Tittel, D. Richter, and A. Fried, "Mid-infrared laser applications in spectroscopy," in *Solid-State Mid-Infrared Laser Sources*, I. T. Sorokina and K. L. Vodopyanov, Eds., pp. 458–529, Springer, Berlin, Heidelberg (2003).
5. A. V. Sokolov, "Applications of coherent Raman scattering," in *Extreme Photonics & Applications*, T. J. Hall, S. V. Gaponenko, and S. A. Paredes, Eds., pp. 75–93, Springer, Netherlands (2010).
6. J. P. Coates, "A practical approach to the interpretation of infrared spectra," in *Encyclopedia of Analytical Chemistry*, R. A. Meyers, Ed., pp. 10815–10837, J. Wiley & Sons Ltd., Chichester, United Kingdom (2000).
7. A. Schliesser, N. Picque, and T. W. Hansch, "Mid-infrared frequency combs," *Nat. Photonics* **6**(7), 440–449 (2012).
8. L.S. Rothman et al., "HITEMP, the high-temperature molecular spectroscopic database," *J. Quant. Spectrosc. Radiat. Transf.* **111**, 2139–2150 (2010).
9. E. H. Wishnow et al., "Mid-infrared interferometry with high spectral resolution," *Proc. SPIE* **7734**, 773409 (2010).
10. Th. Udem, R. Holzwarth, and T. W. Hansch, "Optical frequency metrology," *Nature* **416**(6877), 233–237 (2002).
11. S. T. Cundiff and J. Ye, "Colloquium: femtosecond optical frequency combs," *Rev. Mod. Phys.* **75**(1), 325–342 (2003).
12. D. J. Jones et al., "Carrier-envelope phase control of femtosecond mode-locked lasers and direct optical frequency synthesis," *Science* **288**(5466), 635–639 (2000).
13. Y. R. Shen, *The Principles of Nonlinear Optics*, Wiley, New York (1984).
14. R. W. Boyd, *Nonlinear Optics*, Academic Press, San Diego (2003).
15. A. Newell and J. Moloney, *Nonlinear Optics*, Westview Press, Boulder, Colorado (2003).
16. T. Brabec and F. Krausz, "Nonlinear optical pulse propagation in the single-cycle regime," *Phys. Rev. Lett.* **78**(17), 3282–3285 (1997).
17. J. A. Armstrong et al., "Interactions between light waves in a nonlinear dielectric," *Phy. Rev.* **127**(6), 1918–1939 (1962).
18. E. Harris, "Tunable optical parametric oscillators," *Proc. IEEE* **57**(12), 2096–2113 (1969).
19. R. L. Byer, "Optical parametric oscillators," in *Quantum Electronics, Nonlinear Optics*, H. Rabin and C. L. Tang, Eds., Vol. 1, pp. 587–701, Academic, New York (1975).
20. F. Träger, *Handbook of Laser and Optics*, Springer, New York (2007).
21. P. D. Maker et al., "Effects of dispersion and focusing on the production of optical harmonics," *Phys. Rev. Lett.* **8**(1), 21 (1962).
22. R. Paschotta, *Encyclopedia of Laser Physics and Technology*, Wiley-VCH (2008).
23. G. Dmitriev, G. G. Gurzadyan, and D. N. Nikogosyan, *Handbook of Nonlinear Optical Crystals*, Springer, Berlin, Heidelberg (1991).
24. P. Di Trapani et al., "Matching of group velocities in three-wave parametric interaction with femtosecond pulses and application to traveling-wave generators," *J. Opt. Soc. Am. B* **12**(11), 2237–2244 (1995).
25. K. Moutzouris et al., "Efficient second-harmonic generation in birefringently phase-matched GaAs/Al2O3 waveguides," *Opt. Lett.* **26**(22), 1785–1787 (2001).
26. D. H. Jundt, "Temperature-dependent Sellmeier equation for the index of refraction, ne, in congruent lithium niobate," *Opt. Lett.* **22**(20), 1553–1555 (1997).
27. A. Bruner et al., "Temperature-dependent Sellmeier equation for the refractive index of stoichiometric lithium tantalate," *Opt. Lett.* **28**(3), 194–196 (2003).
28. M. D. Ewbank, M. J. Rosker, and G. L. Bennett, "Frequency tuning a mid-infrared optical parametric oscillator by the electro-optic effect," *J. Opt. Soc. Am. B* **14**(3), 666–671 (1997).
29. K. Kato, "Parametric oscillation at 3.2 μm in KTP pumped at 1.064 μm," *IEEE J. Quantum Electron.* **27**(5), 1137–1139 (1991).
30. Q. Fu, G. Mak, and H. M. van Driel, "High-power, 62-fs infrared optical parametric oscillator synchronously pumped by a 76-MHz Ti:sapphire laser," *Opt. Lett.* **17**(14), 1006–1008 (1992).

31. W. S. Pelouch, P. E. Powers, and C. L. Tang, "Ti:sapphire-pumped, high-repetition-rate femtosecond optical parametric oscillator," *Opt. Lett.* **17**(15), 1070–1072 (1992).
32. K. Zhong et al., "High-pulse-energy high-efficiency mid-infrared generation based on KTA optical parametric oscillator," *Appl. Phys. B* **100**(4), 749–753 (2010).
33. R. F. Wu et al., "Multiwatt mid-IR output from a Nd:YALO laser pumped intracavity KTA OPO," *Opt. Express* **8**(13), 694–698 (2001).
34. F. Bai et al., "Theoretical and experimental studies on output characteristics of an intracavity KTA OPO," *Opt. Express* **20**(2), 807–815 (2012).
35. J. Y. Zhang et al., "Optical parametric generation and amplification in barium borate and lithium triborate crystals," *J. Opt. Soc. Am. B* **10**(9), 1758–1764 (1993).
36. J. Hong et al., "Broadly tunable femtosecond pulse generation in the near and mid-infrared," *Appl. Opt.* **36**(9), 1894–1897 (1997).
37. A. Hemming et al., "99 W mid-IR operation of a ZGP OPO at 25% duty cycle," *Opt. Express* **21**(8), 10062–10069 (2013).
38. Ab. F. Nieuwenhuis et al., "Mid-infrared ZGP optical parametric oscillator directly pumped by a lamp-pumped, Q-switched Cr,Tm,Ho:YAG laser," *Proc. SPIE* **6455**, 645518 (2007).
39. K. L. Vodopyanov et al., "$AgGaS_2$ optical parametric oscillator continuously tunable from 3.9 to 11.3 μm," *Appl. Phys. Lett.* **75**(9), 1204–1206 (1999).
40. S. Chandra et al., "Continuously tunable, 6–14 μm silver-gallium selenide optical parametric oscillator pumped at 1.57 μm," *Appl. Phys. Lett.* **71**(5), 584–586 (1997).
41. R. G. Wenzel and G. P. Arnold, "Parametric oscillator: HF oscillator-amplifier pumped CdSe parametric oscillator tunable from 14.1 μm to 16.4 μm," *Appl. Opt.* **15**(5), 1322–1326 (1976).
42. E. Pelletier et al., "Mid-infrared optical parametric amplifier based on a LGSe crystal and pumped at 1.6 μm," *Opt. Express* **20**(25), 27456–27464 (2012).
43. J. A. Armstrong et al., "Interactions between light waves in a nonlinear dielectric," *Phys. Rev.* **127**(6), 1918–1939 (1962).
44. R. L. Byer, "Quasi-phasematched nonlinear interactions and devices," *J. Nonlinear Opt. Phys. Mater.* **6**(4), 549–592 (1997).
45. G. D. Boyd and C. K. N. Patel, "Enhancement of optical second-harmonic generation (SHG) by reflection phase matching in ZnS and GaAs," *Appl. Phys. Lett.* **8**(12), 313–315 (1966).
46. H. Komine et al., "Quasi-phasematched second-harmonic generation by use of a total-internal-reflection phase shift in gallium arsenide and zinc selenide plates," *Opt. Lett.* **23**(9), 661–663 (1998).
47. R. Haidar et al., "Quasiphase-matched difference frequency generation (8–13 μm) in an isotropic semiconductor using total reflection," *Appl. Phys. Lett.* **82**(8), 1167–1169 (2003).
48. R. Haidar, P. Kupecek, and E. Rosencher, "Nonresonant quasi-phase matching in GaAs plates by Fresnel birefringence," *Appl. Phys. Lett.* **83**(8), 1506–1508 (2003).
49. D. Feng et al., "Enhancement of second harmonic generation in LiNbo3 crystals with periodic laminar ferroelectric domains," *Appl. Phys. Lett.* **37**(7), 607–609 (1980).
50. S. Zhu, Y. Y. Zhu, and N. B. Ming, "Quasi-phase-matched third-harmonic generation in a quasiperiodic optical superlattice," *Science* **278**(5339), 843–846 (1997).
51. B. E. A. Saleh and M. C. Teich, *Fundamentals of Photonics*, 2nd ed., Wiley, New York (2007).
52. A. Henderson and R. Stafford, "Low threshold, singly-resonant CW OPO pumped by an all-fiber pump source," *Opt. Express* **14**(2), 767–772 (2006).
53. P. S. Kuo and M. M. Fejer, "Microstructured semiconductors for mid-infrared nonlinear optics," in *Mid-Infrared Coherent Sources and Applications*, M. Ebrahim-Zadeh and I. T. Sorokina, Eds., pp. 149–168, Springer, Dordrecht, The Netherlands (2008).
54. P. S. Kuo, "Thick film, orientation-patterned gallium arsenide for nonlinear optical frequency conversion," PhD Dissertation, Stanford University (2008).
55. D. Zheng et al., "Diffusion bonding of GaAs wafers for nonlinear optics applications." *J. Electrochem. Soc.* **144**(4), 1439–1441 (1997).
56. B. J. Perrett et al., "Optical parametric amplification of mid-infrared radiation using multi-layer glass-bonded QPM GaAs crystals," *Proc. SPIE* **6455**, 64550A (2007).
57. K. C. Rustagi, S. C. Mehendale, and S. Meenakshi, "Optical frequency conversion in quasi-phase-matched states of nonlinear crystals," *IEEE J. Quantum Electron.* **18**(6), 1029–1041 (1982).
58. S. J. B. Yoo et al., "Quasi-phase-matched second harmonic generation in AlGaAs waveguides with periodic domain inversion achieved by wafer bonding," *Appl. Phys. Lett.* **66**(25), 3410–3412 (1995).
59. K. L. Vodopyanov et al., "Optical parametric oscillation in quasi-phase-matched GaAs," *Opt. Lett.* **29**(16), 1912–1914 (2004).
60. C. Kieleck et al., "High-efficiency 20–50 kHz mid-infrared orientation-patterned GaAs optical parametric oscillator pumped by a 2 μm holmium laser," *Opt. Lett.* **34**(3), 262–264 (2009).
61. W. C. Hurlbut et al., "Multiphoton absorption and nonlinear refraction of GaAs in the mid-infrared," *Opt. Lett.* **32**(6), 668–670 (2007).
62. R. K. Feaver, R. D. Peterson, and P. E. Powers, "Longwave-IR optical parametric oscillator in orientation-patterned GaAs pumped by a 2 μm Tm,Ho:YLF laser," *Opt. Express* **21**(13), 16104–16110 (2013).
63. C. Kieleck et al., "OP-GaAs OPO pumped by 2 μm Q-switched lasers: Tm;Ho:silica fiber laser and Ho:YAG laser," *Proc. SPIE* **7836**, 783607 (2010).
64. D. Creeden et al., "Mid-infrared $ZnGeP_2$ parametric oscillator directly pumped by a pulsed 2 μm Tm-doped fiber laser," *Opt. Lett.* **33**(4), 315–317 (2008).
65. N. Leindecker et al., "Octave-spanning ultrafast OPO with 2.6–6.1 μm instantaneous bandwidth pumped by femtosecond Tm-fiber laser," *Opt. Express* **20**(7), 7046–7053 (2012).
66. K. F. Lee et al., "Carrier envelope offset frequency of a doubly resonant, nondegenerate, mid-infrared GaAs optical parametric oscillator," *Opt. Lett.* **38**(8), 1191–1193 (2013).
67. M. Baudrier-Raybaut et al., "Random quasi-phase-matching in bulk polycrystalline isotropic nonlinear materials," *Nature* **432**(7015), 374–376 (2004).
68. X. Vidal and J. Martorell, "Generation of light in media with a random distribution of nonlinear domains," *Phys. Rev. Lett.* **97**(1), 013902 (2006).
69. E. Andrieux et al., "500 GHz mode-hop-free idler tuning range with a frequency-stabilized singly resonant optical parametric oscillator," *Opt. Lett.* **36**(7), 1212–1214 (2011).
70. S. G. Sabouri, A. Khorsandi, and M. Ebrahim-Zadeh, "Power instability of singly resonant optical parametric oscillators: theory and experiment," *Opt. Express* **20**, 27442–27455 (2012).
71. W. R. Bosenberg et al., "93% pump depletion, 3.5-W continuous-wave, singly resonant optical parametric oscillator," *Opt. Lett.* **21**(25), 1336–1338 (1996).
72. K. Schneider et al., "Toward an optical synthesizer: a single-frequency parametric oscillator using periodically poled $LiNbO_3$," *Opt. Lett.* **22**(17), 1293–1295 (1997).
73. D. J. M. Stothard, M. Ebrahimzadeh, and M. H. Dunn, "Low-pump-threshold continuous-wave singly resonant optical parametric oscillator," *Opt. Lett.* **23**(24), 1895–1897 (1998).
74. M. E. Klein et al., "Singly resonant continuous-wave optical parametric oscillator pumped by a diode laser," *Opt. Lett.* **24**(16), 1142–1144 (1999).
75. K. Devi et al., "Antiresonant ring output-coupled continuous-wave optical parametric oscillator," *Opt. Express* **20**(17), 19313–19321 (2012).
76. J. Falk, "Instabilities in the doubly resonant parametric oscillator: a theoretical analysis," *IEEE J. Quantum Electron.* **7**(6), 230–235 (1971).
77. C. D. Nabors et al., "Efficient, single-axial-mode operation of a monolithic $MgO:LiNbO_3$ optical parametric oscillator," *Opt. Lett.* **14**(20), 1134–1136 (1989).
78. L. Xu, S. Zhang, and W. Chen, "Tm:YLF laser-pumped periodically poled MgO-doped congruent $LiNbO_3$ crystal optical parametric oscillators," *Opt. Lett.* **37**(4), 743–745 (2012).
79. M. E. Klein et al., "Diode-pumped continuous-wave widely tunable optical parametric oscillator based on periodically poled lithium tantalate," *Opt. Lett.* **23**(11), 831–833 (1998).
80. J.-J. Zondy et al., "Output power optimization of continuous-wave, mid-infrared AgGaS2 doubly/triply resonant optical parametric oscillator," presented at *Advanced Solid State Lasers*, paper WB6, Optical Society of America, Boston, Massachusetts (31 January 1999).
81. J. Teja and N. Wong, "Twin-beam generation in a triply resonant dual-cavity optical parametric oscillator," *Opt. Express* **2**(3), 65–71 (1998).
82. I. Breunig, D. Haertle, and K. Buse, "Continuous-wave optical parametric oscillators: recent developments and prospects," *Appl. Phys. B* **105**(1), 99–111 (2011).
83. M. Ebrahim-Zadeh et al., "Breakthroughs in photonics 2012: breakthroughs in optical parametric oscillators," *IEEE Photon. J.* **5**(2), 700105 (2013).
84. C. Diederichs et al., "Parametric oscillation in vertical triple microcavities," *Nature* **440**(7086), 904–907 (2006).
85. C. Y. Wang et al., "Mid-infrared optical frequency combs at 2.5 μm based on crystalline microresonators," *Nat. Commun.* **4**, 1345 (2013).
86. S. E. Harris, "Proposed backward wave oscillation in the infrared," *Appl. Phys. Lett.* **9**(3), 114–116 (1966).
87. C. Canalias and V. Pasiskevicius, "Mirrorless optical parametric oscillator," *Nat. Photonics* **1**(8), 459–462 (2007).
88. J. B. Khurgin, "Optical parametric oscillator: Mirrorless magic," *Nat. Photonics* **1**(8), 446–447 (2007).
89. D. G. Lancaster et al., "Real-time measurements of trace gases using a compact difference-frequency-based sensor operating at 3.5 μm," *Appl. Phys. B* **67**(3), 339–345 (1998).
90. Z. G. Guan et al., "Vertical lidar sounding of atomic mercury and nitric oxide in a major Chinese city," *Appl. Phys. B* **101**(1–2), 465–470 (2010).
91. F. Kuhnemann et al., "Photoacoustic trace-gas detection using a cw single-frequency parametric oscillator," "Photoacoustic trace-gas detection using a cw single-frequency parametric oscillator," *Appl. Phys. B* **66**(6), 741–745 (1998).

92. M. W. Todd et al., "Application of mid-infrared cavity-ringdown spectroscopy to trace explosives vapor detection using a broadly tunable (6–8 μm) optical parametric oscillator," *Appl. Phys. B* **75**(2–3), 367–376 (2002).
93. Y. He, M. Hippler, and M. Quack, "High-resolution cavity ringdown absorption spectroscopy of nitrous oxide and chloroform using a near infrared cw diode laser," *Chem. Phys. Lett.* **289**(5–6), 527–534 (1998).
94. D. Zhao et al., "Mid-infrared continuous wave cavity ring-down spectroscopy of a pulsed hydrocarbon plasma," *Chem. Phys. Lett.* **565**, 132–137 (2013).
95. B. A. Paldus and A. A. Kachanov, "An historical overview of cavity-enhanced methods," *Can. J. Phys.* **83**(10), 975–999 (2005).
96. A. Marian et al., "United time-frequency spectroscopy for dynamics and global structure," *Science* **306**(5704), 2063–2068 (2004).
97. F. Adler et al., "Phase-stabilized, 1.5 W frequency comb at 2.8–4.8 μm," *Opt. Lett.* **34**(9), 1330–1332 (2009).
98. M. W. Haakestad et al., "Intracavity trace molecular detection with a broadband mid-IR frequency comb source," *J. Opt. Soc. Am. B* **30**(3), 631–640 (2013).
99. A. Marandi et al., "Coherence properties of a broadband femtosecond mid-IR optical parametric oscillator operating at degeneracy," *Opt. Express* **20**(7), 7255–7262 (2012).
100. T. Lang et al., "High power ultra-widely tuneable femtosecond pulses from a non-collinear optical parametric oscillator (NOPO)," *Opt. Express* **20**(2), 912–917 (2012).
101. M. J. Thorpe et al., "Broadband cavity ringdown spectroscopy for sensitive and rapid molecular detection," *Science* **311**(5767), 1595–1599 (2006).
102. M. J. Thorpe and J. Ye, "Cavity-enhanced direct frequency comb spectroscopy," *Appl. Phys. B* **91**(3–4), 397–414 (2008).
103. F. Adler et al., "Cavity-enhanced direct frequency comb spectroscopy: technology and applications," *Annu. Rev. Anal. Chem.* **3**, 175–205 (2010).
104. M. J. Thorpe et al., "Cavity-enhanced optical frequency comb spectroscopy: application to human breath analysis," *Opt. Express* **16**(4), 2387–2397 (2008).
105. M. W. Haakestad et al., "Intracavity trace molecular detection with a broadband mid-IR frequency comb source," *J. Opt. Soc. Am. B* **30**(3), 631–640 (2013).
106. D. Richter et al., "Field measurements of volcanic gases using tunable diode laser based mid-infrared and Fourier transform infrared spectrometers," *Opt. Lasers Eng.* **37**(2–3), 171–186 (2002).
107. L. B. Flanagan and J. R. Ehleringer, "Ecosystem-atmosphere CO_2 exchange: interpreting signals of change using stable isotope ratios," *Trend Ecol. Evol.* **13**(1), 10–14 (1998).
108. F. Keilmann, Ch. Gohle, and R. Holzwarth, "Time-domain mid-infrared frequency-comb spectrometer," *Opt. Lett.* **29**(13), 1542–1544 (2004).
109. I. Coddington, W. C. Swann, and N. R. Newbury, "Coherent multiheterodyne spectroscopy using stabilized optical frequency combs," *Phys. Rev. Lett.* **100**(1), 013902 (2008).
110. F. Zhu et al., "Real-time dual frequency comb spectroscopy in the near infrared," *Appl. Phys. Lett.* **102**(12), 121116 (2013).
111. F. Adler et al., "Mid-infrared Fourier transform spectroscopy with a broadband frequency comb," *Opt. Express* **18**(21), 21861–21872 (2010).
112. Z. Zhang, T. Gardiner, and D. T. Reid, "Mid-infrared dual-comb spectroscopy with an optical parametric oscillator," *Opt. Lett.* **38**(16), 3148–3150 (2013).
113. C.-H. Li et al., "A laser frequency comb that enables radial velocity measurements with a precision of 1 cm s^{-1}," *Nature* **452**(7178), 610–612 (2008).
114. T. Steinmetz et al., "Laser frequency combs for astronomical observations," *Science* **321**(5894), 1335–1337 (2008).
115. O. Kokabee, A. Esteban-Martin, and M. Ebrahim-Zadeh, "Extended-cavity, tunable, GHz-repetition-rate femtosecond optical parametric oscillator pumped at 76 MHz," *Opt. Express* **17**(18), 15635–15640 (2009).
116. T. Ideguchi et al., "Coherent Raman spectro-imaging with laser frequency combs," *Nature* **502**(7471), 355–358 (2013).
117. A. Esteban-Martin et al., "Frequency-modulation-mode-locked optical parametric oscillator," *Opt. Lett.* **37**(1), 115–117 (2012).
118. K. Devi, S. Ch. Kumar, and M. Ebrahim-Zadeh, "Mode-locked, continuous-wave, singly resonant optical parametric oscillator," *Opt. Lett.* **37**(18), 3909–3911 (2012).
119. T. J. Kippenberg, R. Holzwarth, and S. A. Diddams, "Microresonator-based optical frequency combs," *Science* **332**(6029), 555–559 (2011).
120. B. Guo et al., "Laser-based mid-infrared reflectance imaging of biological tissues," *Opt. Express* **12**(1), 208–219 (2004).
121. V. A. Serebryakov et al., "Medical applications of mid-IR lasers. Problems and prospects," *J. Opt. Technol.* **77**(1), 6–17 (2010).

Jiahui Peng received his BS in optics from Nankai University, and his PhD in physics from Texas A&M University. After working as a postdoctoral fellow in NRC-uOttawa Joint Attosecond Science Laboratory, he is working as a research scientist at IMRA America Inc.